



Blue-emitting thermoreversible oligourethane gelators with aggregation-induced emission properties

Nan Jiang,^a Dongxia Zhu,^{*a} Zhongmin Su^{*a} and Martin R. Bryce^{*b}

Received 00th January 20xx,
Accepted 00th January 20xx

DOI: 10.1039/x0xx00000x

www.rsc.org/

Blue-emitting gels are scarce, especially oligomeric/polymeric systems. Here, a series of 4,4'-sulfonyldiphenol (SDP) based oligourethane derivatives (OUs), namely **OUHDI**, **OUHMDI** and **OUTDI** based on 1,6-hexamethylene diisocyanate, 4,4'-methylenebis(cyclohexyl isocyanate) and 2,4-diisocyanatotoluene, respectively, were rationally designed and obtained by simple procedures. The new oligomers all display aggregation-induced blue fluorescence and upon gelation they achieve enhanced bright deep-blue emission as a result of interchain hydrogen bonding and oxygen cluster interactions. The OUs show spontaneous thermoreversible gelation in solvents which possess hydrogen-bond receptor units (C=O or S=O) which facilitate self-assembly of the OU chains into nanotubes. The oligourethane gels (**OUGs**) possess excellent ability for resisting external stress while at the same time exhibiting a distinct viscous flow state. The results illustrate that heteroatomic non-conjugated oligomers with advantageous hydrogen bonding interactions and oxygen clusters provide an efficient route to photoluminescent blue-emitting gels. The thermoreversible **OUGs** with excellent mechanical properties have been exploited to make sticky coatings, transparent films and a blue fluorescent molded shape using simple fabrication processes.

Introduction

Photoluminescent (PL) gels are widely used in optoelectronic devices,¹ chemical/biochemical sensors,² biological applications,³ and other fields.⁴⁻⁶ A drawback of many PL gel systems, such as metal-organic frameworks (MOFs),⁷ rare-earth luminescent materials,⁸ metallic coordination polymers,⁹ carbon dots (CDs),¹⁰ and low molecular weight gelators¹¹ is that most of them include expensive or toxic heavy metals and have poor solution processability, greatly limiting their practical applications. By comparison, polymer/copolymer/oligomer gelators offer several advantages, such as low cost, ease of synthesis, and they generally possess good responsive functionalities to the environment or external stimuli.¹²⁻¹⁴ Based on the manner of cross-linking, polymer gelators are categorized as physical gels (which rely on physical interactions such as helical structure,

crystallite structure, hydrogen bonding or electrostatic forces, and so on) and chemical gels (which rely on covalent bonds).¹⁵ Chemical gels generally have high stability and mechanical strength and are commonly used as structural materials. In contrast, physical gels, which can undergo sol-gel-sol reversible transitions in response to changing external conditions (such as temperature and stress) have a promising future¹⁶⁻¹⁸ and are gaining more widespread attention in response to public requirements for intelligent materials.¹⁹⁻²⁰

Traditional conjugated chromophores suffer from aggregation-caused quenching (ACQ), which results in a low fluorescence quantum yield, leading to limitations in their practical luminescence applications in the solid state.²¹⁻²³ Hence, in order to make full use of PL gels in real-life applications, a prerequisite is synthesizing gelators with excellent photoluminescence properties in the aggregation state. In this regard, molecules which display clustering-triggered emission²⁴⁻²⁵ or aggregation-induced emission (AIE)²⁶⁻³⁰ are providing new research opportunities.

Conventional PL gelators with typical polycyclic π -conjugated chromophoric units usually have strong π - π stacking interactions and lower energy emission bands in the green, yellow or red regions.^{6,10,31-33} Only a few small-molecule gels with blue emission have been reported.³⁴⁻³⁷ In particular, only one example of a blue-emitting polyurethane gelator has been reported. This is a specialized case where the blue emission is

^a Key Laboratory of Nanobiosensing and Nanobioanalysis at Universities of Jilin Province, Department of Chemistry, Northeast Normal University, 5268 Renmin Street, Changchun, Jilin Province 130024, P.R. China. E-mail: zhudx047@nenu.edu.cn; zmsu@nenu.edu.cn

^b Department of Chemistry, Durham University, Durham, DH1 3LE, UK. E-mail: m.r.bryce@durham.ac.uk

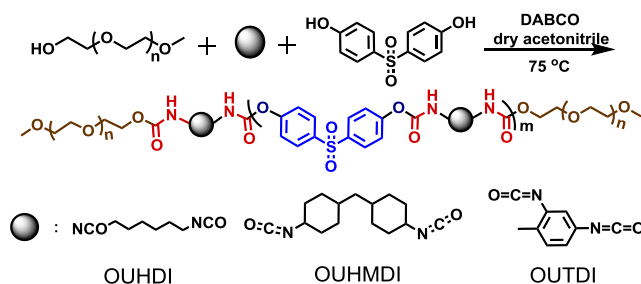
† Electronic Supplementary Information (ESI) available: Experimental details, ¹H NMR spectra and photophysical properties. See DOI: 10.1039/x0xx00000x

assigned to triarylamine substituents in the polymer films after electrochemical oxidation.³⁸

We recognized that electron-rich heteroatoms (O, N or S) or unsaturated subgroups (C=O or S=O) are seldom used in the design of PL gelators. These unusual chromophores should effectively block strong electronic coupling, and also avoid strong π - π stacking interactions, and thereby benefit both the AIE behavior and blue emission simultaneously.³⁹⁻⁴⁰ Therefore, developing new types of PL gelators is desirable and a challenge to make up for the lack of blue-emitting gelators. Polyurethanes are highly appealing on account of their excellent thermoplasticity, chain flexibility and structural versatility. They are widely used in many applications such as textiles and apparels, fibers, and adhesives.⁴¹⁻⁴⁴ Moreover, they are easy to prepare, low cost, and environmentally-friendly compared with many traditional organic materials. We have recently reported that non-conjugated polyurethanes show excellent luminescent behavior due to the presence of multiple C=O and N-H groups in the chains.²⁵ We hypothesized that the introduction of more heteroatoms into non-conjugated polyurethane chains should be a good way to achieve blue-emitting gelators based on the following design criteria: (i) Increase the content of hydrogen-bond donors/acceptors among the main chains. (ii) Combine other non-covalent interactions, such as van der Waals forces, which could favour strong interactions among the flexible and soft polyurethane chains. (iii) Incorporate a solvent with hydrogen-bond receptor groups to assist the realization of a blue-emitting gel.

Inspired by the above considerations, a series of novel blue-emitting oligourethanes, **OUHDI**, **OUHMDI** and **OUTDI** were rationally designed and synthesized (Scheme 1). In the present series three diisocyanates with different chemical structures and spatial configuration were inserted separately for comparing changes in self-assembly and mechanical properties of the OUs. A special structural feature is that all three OU derivatives contain the aromatic 4,4'-sulfonyldiphenol (SDP) unit in the backbone. The introduction of O=S=O units provides two advantages over previous urethane derivatives: (i) There are more possibilities for forming oxygen clusters, by spacial overlap and communication between electron lone pairs on the oxygen atoms; and (ii) interchain hydrogen bonding involving O=S=O units is available to enhance interchain interactions. These combined properties serve to limit the internal bond rotations within the OU chains, thereby enhancing their photophysical properties in aggregation states.

The AIE properties, facile H-bonding-driven self-assembly, gelation and the mechanical properties of **OUHDI**, **OUHMDI** and **OUTDI** have been investigated in detail by Fourier transform infrared spectroscopy (FTIR), transmission electron microscopy (TEM) and dynamic viscoelastic experiments. The physical PL gelator applications based on the thermoreversibility properties of **OUHDI** have been successfully exploited to make sticky coatings, transparent films and a blue fluorescent molded shape.



Scheme 1 Synthetic routes for **OUHDI**, **OUHMDI** and **OUTDI** and structures of the diisocyanate precursors.

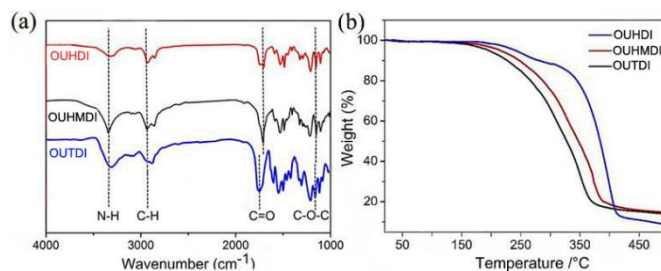


Fig. 1 (a) FTIR spectra of **OUHDI**, **OUHMDI** and **OUTDI**. (b) TGA plots of the OUs.

Results and discussion

Synthesis and Characterization

The OUs were synthesized in a single-pot reaction (Scheme 1) by reacting 4,4'-sulfonyldiphenol (SDP), the appropriate diisocyanate and DABCO in anhydrous acetonitrile. Finally, adding polyethylene glycol monomethyl ether caused the clear solution to turn viscous. The products **OUHDI**, **OUHMDI** and **OUTDI** were purified using counter precipitation methods. The M_w values of 4192, 1749 and 2775 g mol^{-1} , respectively, determined by ^1H NMR analysis, established that the products should be classified as oligomeric, rather than polymeric (Fig. S1-S3). The detailed synthetic methods and ^1H NMR characterization are reported in the Supporting Information. FTIR spectra of the OUs in the solid-state show bands at 1712 cm^{-1} and 3342 cm^{-1} corresponding to $\nu(\text{C}=\text{O})$ and $\nu(\text{N}-\text{H})$ stretching vibrations, establishing the formation of amide bonds in the backbone (Fig. 1a). Thermogravimetric analysis (TGA) (Fig. 1b) shows that the OUs decompose at $249\text{ }^\circ\text{C}$, $224\text{ }^\circ\text{C}$ and $206\text{ }^\circ\text{C}$, respectively, demonstrating excellent thermal stability. The relatively lower heat tolerance of **OUTDI** is ascribed to the rigid and asymmetric structure of the units derived from the 2,4-tolylene diisocyanate precursor, which lowers the crystallinity of **OUTDI**.

AIE Properties

Since bright luminescence is observed in the solid and highly concentrated solution states of the three OUs, their AIE properties were explored at room temperature. The absorption spectrum of **OUHDI** in the solid-state (Fig. S4) shows a major peak at 265 nm corresponding to a π - π^* transition, supporting the existence of conjugated aromatic rings from the diphenylsulfone unit.⁴⁵ As

shown in Fig. 2a, **OUHDI** exhibits faint emission in 10^{-5} M acetone solution. However, the PL intensity gradually increases with addition of water which is a poor solvent for **OUHDI**. When the water fraction exceeded 60% the PL intensity enhanced dramatically. In the case of 90% volume fraction of water, the relative quantum yield (η) of **OUHDI** is 20%, which is 200 times higher than the value in pure acetone ($\eta = 0.01$). To gain more insights into the luminescence mechanism, the concentration-dependent emission spectra of **OUHDI** were recorded in pure acetone solution (Fig. 2b). The concentrations of **OUHDI** were chosen within the range of 0.1 to 20 mg/mL, and with increasing the concentration, strikingly enhanced emission was observed, and new emission peaks appeared. These data are explained by the non-conjugated OU chains approaching each other and interacting with discrete carbonyl units gathered to forming carbonyl clusters, thereby generating various aggregates which favour the emission.⁴⁶

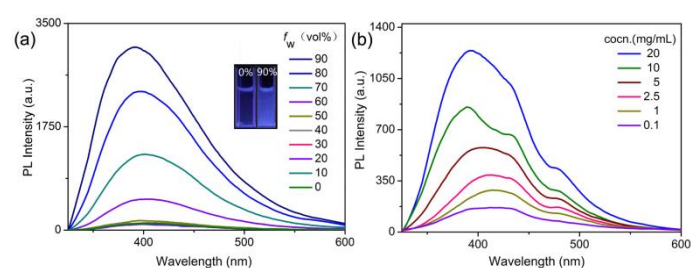


Fig. 2 (a) PL spectra of **OUHDI** (10^{-5} M) in acetone-water mixtures with different water fractions (0-90% v/v) at room temperature. (b) PL spectra of **OUHDI**/acetone with different concentrations.

Transmission electron microscopy (TEM) experiments also confirmed that aggregated nanoparticles are formed in the mixed acetone and water solutions (Fig. S5). All the above results demonstrate that **OUHDI** is an AIE-active oligomer.

Gelation and Nanotubular Assembly

Self-assembly of **OUHDI** was tested in dimethyl formamide (DMF) at 8 wt% concentration (according to the repeat unit). For these studies 8 wt% of gelators was used to guarantee some mechanical strength, which is better for dynamic rheological tests and applications. **OUHDI** was soluble upon heating, and upon subsequent cooling to room temperature the solution gradually became viscous and after 48 h produced a blue-emitting gel with a critical gelation concentration (CGC) of 3.5 wt% and T_{gel} of 63 °C at CGC. The **OUHDI** solid showed blue emission at $\lambda_{max} = 409$ nm when excited at $\lambda_{ex} = 365$ nm, while **OUHDI** gel showed a visibly stronger blue emission at $\lambda_{max} = 471$ nm ($\lambda_{ex} = 365$ nm) with a significant shift of 62 nm with respect to the solid sample (Fig. S6). This shift can be attributed to the more entangled and aggregated chains in the gel state due to the increased number of hydrogen-bond receptors compared to the solid state. The stability of the **OUHDI** was verified by a stable-to-inversion of the vial method (Fig. S7d). Such facile and reversible gelation ability of **OUHDI** was tested in other solvents, and the increase of self-assembly was observed only in dimethyl formamide (DMF), dimethyl acetamide (DMAC), and dimethyl sulfoxide (DMSO), as shown in the Table S1. Notably these three solvents all have hydrogen-bond receptor

units (C=O or S=O) providing evidence that H-bonding is strongly involved in the gelation process. Interestingly, gelation properties were found to be concentration-dependent and time-dependent (Fig. S7a). Gelation occurred more rapidly at higher concentrations of the OU derivative, consistent with the existence of interchain interactions. TEM images revealed contrasting morphologies between a freshly prepared solution and an aged gel of **OUHDI**. The spherical and sheet nanoaggregates that formed initially (Fig. S7b) turned into an entangled one-dimensional network structure (Fig. S7c) upon ageing, thus explaining the observed several tens of hours of slow gelation.

The self-assembly behavior, and the macroscopic gel characteristics of **OUHDI** are shown in Fig. 3. The microscopic gel formation process was investigated by TEM with an incremental increase in concentration (0.0064 wt% to 0.8 wt%). TEM images of **OUHDI** in DMF with increasing concentrations revealed microstructural features from a discrete vesicular precipitate to gradually merged nanospheres and ultimately to nanotubular structures (Fig. 3a-d) showing macroscopic gel characteristics (Fig. 3e). Nanotubular structures of **OUHMDI** and **OUTDI** in DMF were also observed by TEM (Fig. S8a and S8b). The stepwise self-assembly is attributed to H-bonding interactions among the urethane and sulfone groups to generate nanotubular structures via a polymersome-like intermediate (Scheme 2).⁴⁷⁻⁵¹

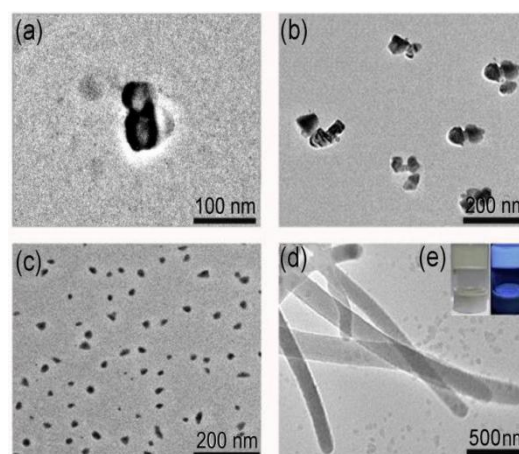


Fig. 3 TEM images of nanoaggregates and nanotubes of **OUTDI** formed in DMF solution (a) 0.0064 wt% (b) 0.064 wt% (c) 0.64 wt% (d) 0.8 wt% and (e) Images of **OUTDI** gel (c = 8 wt%) in DMF in daylight (left) and under UV light (right) ($\lambda_{ex} = 365$ nm).

Spectroscopic Studies

To correlate macroscopic properties and molecular structure, FTIR and fluorescence experiments were conducted. FTIR spectra of **OUHDI** in gel and solid states were compared (Fig. 4a). The peaks characteristic of the -C=O bond of the OU chains shifted to lower wavenumber by 56 cm^{-1} (1712 to 1656 cm^{-1}) in DMF, indicating strong H-bonding interactions between the OU chains in the gel state.⁵² Moreover, the stretching frequency of -CH₂- groups moved to significantly higher wavenumbers (2998 and 2913 cm^{-1} , respectively) in the gel state compared to the solid state (2933 and

2858 cm^{-1} , respectively), indicating ordered packing of $-\text{CH}_2-$ units in the formation of nanotubes.⁵³ FTIR spectroscopic data for **OUHMDI** and **OUTDI** in gel and solid states gave directly comparable results to **OUHDI** (Figs. S8c and S8d). To investigate the influence of the new structural feature of $\text{O}=\text{S}=\text{O}$ units in the molecular design of the **OUGs**, FTIR spectra were recorded for two concentrations of **OUHDI** in D_2O (Fig. 4b). At the higher concentration the peaks characteristic of the $\text{S}=\text{O}$ group shifted to a lower wavenumber by 12 cm^{-1} (1448 to 1436 cm^{-1}) indicating H-bonding interactions of the $\text{S}=\text{O}$ units. Therefore, we conclude that $\text{O}=\text{S}=\text{O}$ units are beneficial in promoting gelation. Besides, in the presence of urea, which can denature and destroy the assembly of H-bonds among OU chains by forming H-bonds with the amide groups,⁵⁴ the **OUHDI** gel in DMF was converted to a sol state (Fig. S9-S11) further suggesting H-bonding mediated assembly. Additional insights into the relationship between gelation properties and molecular structure were obtained from the enthalpy of melting (ΔH_m) by the Schroeder-van Laar equation.

$$\ln[\text{gelator}] = \frac{\Delta H_m}{RT_{\text{gel}}} + \text{constant}$$

In this equation, ΔH_m and T_{gel} represent the enthalpy of melting and the melting temperature of gel-to-sol, respectively. In Fig. 5a, T_{gel} vs. $[\text{gelator}]$ plots of **OUHDI**, **OUHMDI**, and **OUTDI** all showed a stable increase in T_{gel} with an increase of the gelators' concentration. This could be because at higher concentration the gel networks need longer periods of gradual dissolution time, reflecting the gelation caused by self-aggregation and self-assembly through various non-covalent interactions, such as hydrogen bonds, π - π stacking, and van der Waals interactions. Arrhenius plots of $\ln[\text{gelator}]$ vs. $1/T_{\text{gel}} \text{ K}^{-1}$ gave linear plots from which ΔH_m values were calculated to be 20.3, 18.4, and 15.0 kJ/mol, respectively (Fig. 5b and Table S2). In summary, gelation of the OUs occurs at room temperature and the gels turn into sols at 50-99 °C; the broad sol-gel-sol thermoresponsive temperature range has outstanding potential in real-life applications.

Mechanical Properties

Mechanical properties of soft materials are very important. How to purposefully adjust the mechanical properties of physical gels is a crucial aspect in the practical utilization of both environment stimuli-responsive and mechanical behaviours.⁵⁵ To assess the mechanical properties of the **OUGs** dynamic rheological data were obtained using strain sweep measurements with a frequency of 1 Hz at 25 °C. The storage modulus (G') and loss modulus (G'') characterized upon the applied stress are shown in Fig. 6a-c and Table S2. As can be seen from Fig. 6a when the stress is $<1.5\%$, the G' of **OUHDI** is $>G''$, indicating a typical gel phase viscoelastic region. When the applied stress was increased, entangled polymer chains in solution were destroyed and became more orderly arrayed. The intersection of the G' and G'' curves represent the gel-sol transition point. Beyond the critical stress value (i.e., yield stress σ) the system showed prevailing viscous behavior and began to flow, $G'' > G'$. **OUHMDI** and **OUTDI** also showed similar rheological behavior. Note that the G' value and yield stress of **OUHDI** gel is

the highest among the three gel samples, confirming its most efficient gelation, which is also established by its high temperature for the gel-to-sol transition. The viscoelastic parameters are influenced by the conformation of the diisocyanate structures; for the **OUHDI** and **OUHMDI** samples the evolution of the viscoelastic values is similar (Fig. 6a and 6b). Although both **OUHDI** and **OUHMDI** have a highly symmetric structure, **OUHDI** has higher viscoelastic parameters as the more linear diisocyanate (HDI) unit is very favourable for strong hydrogen bonding interactions. In contrast **OUTDI** behaves differently (Fig. 6c), as its non-regular (*meta*-linked) structure and poor crystallinity lead to weaker gelation.

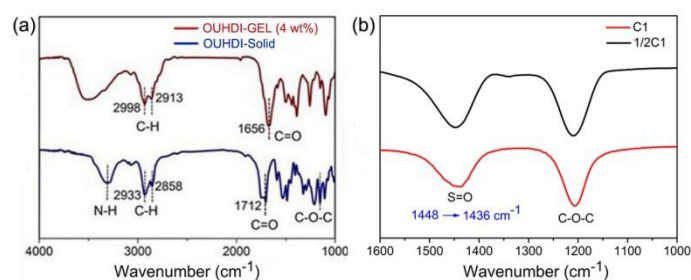
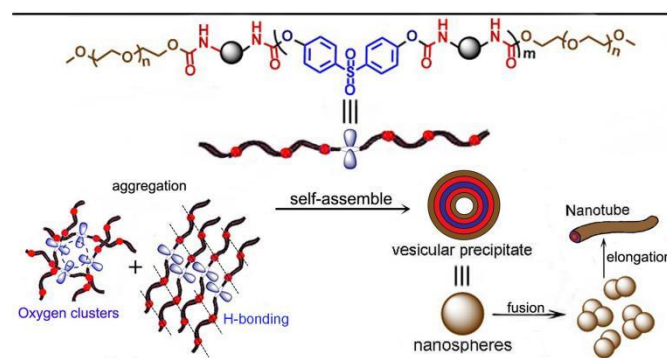


Fig. 4 (a) FTIR spectra of **OUHDI** in solid and gel states. (b) FTIR spectra of **OUHDI** with different concentrations in D_2O ($\text{C1} = 10^{-3} \text{ M}$).



Scheme 2 Proposed model for self-assembly of OUs.

The gel-to-sol transition of the **OUGs** could also be induced by manually shaking a vial containing the gel for about 5 min. These results show that the rheological curing behaviour of **OUGs** makes them suitable materials for the development of advanced composites.

Solution Processability

Excellent solution processability is important for materials which are to be applied in practical applications or device fabrication. Physical gels are easily processed as a result of their reversible gel-sol-gel transitions. Pouring, injection molding, spin-coating and even 3D-printing techniques can be applied to place the sol into containers of almost any size and shape. After gelation, a predetermined shape and size of the gel can be obtained, or further processed into a flexible polymer film. In Fig. 6d, a sticky adhesive **OUHDI** gel was painted onto stereoscopic molds, showing a blue pattern under a UV lamp. Fig. 6e shows a transparent film of **OUHDI** with high optical quality, which was cast on a PTFE board and cut to the required shapes. The

film maintained stable fluorescence performance at room temperature, unless destroyed by dissolving in a highly polar solvent.

To exploit the combined gelation and AIE properties, **OUHDI** gel was placed into a pig-shaped hollow metal mold. The shape of the gel was retained after removal of the mold and the strong blue fluorescence was clearly visible to naked eyes (Fig. 6f). These results demonstrate that these physical gels are highly processable, which is of paramount importance for large-area coating and potential applications such as advanced composites, emissive displays, solid-state lighting or thermal sensing.

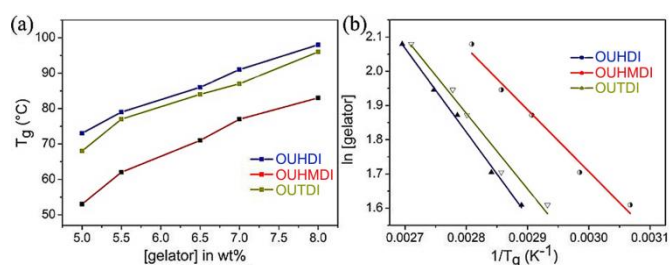


Fig. 5 (a) Variation of T_{gel} as a function of gelator concentration; (b) analysis of the data presented in Fig. 5a with the Schroeder–van Laar equation.

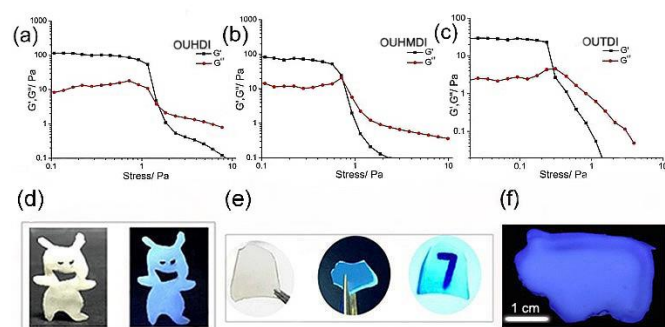


Fig. 6 Variation of G' and G'' as a function of applied stress for (a) **OUHDI**, (b) **OUHMDI** and (c) **OUTDI** gelators in DMF ($c = 8$ wt%). (d) A gel of **OUHDI** painted on molds, under sunlight (left) and under excitation at 365 nm (right). (e) Formation of transparent and stable fluorescent films of **OUHDI** under sunlight (left) and under excitation at 365 nm (right), showing the number seven in the background through the transparent gel. (f) A pig-shaped **OUHDI** gel after removing the hollow metal mold.

Conclusions

To sum up, a series of three heteroatomic non-conjugated blue oligourethane derivatives based on SDP-diol were synthesized and characterized. The introduction of O=S=O units is beneficial for forming oxygen clusters and hydrogen bonding among chains to limit the internal rotations, thus enhancing their photophysical properties in aggregation states. The **OUGs** show enhanced mechanical properties and deep-blue emission in the self-assembled gel state. The **OUGs** show excellent solution processability and can be used to make a sticky coating, transparent films or fixed into a more complex shape while maintaining

excellent optical performance. To explore structure-property relationships three diisocyanates with different chemical structures and spatial configuration were inserted separately for comparing changes in self-assembly and mechanical properties of the OUs. **OUHDI** showed the most efficient thermoreversible gelation in the series due to the high crystallization ability of the higher symmetric linear structure.

This approach of introducing additional heteroatoms into a non-conjugated skeleton, and then combining oxygen cluster and H-bonding interactions, represents a new direction for fabricating deep-blue luminescent gelators for real-life applications. Unconventional stable blue chromophores are highly sought after for practical applications in high-quality displays. Blue emitters should possess a wide band-gap (E_g), making it difficult to design blue emitters based on traditional phosphorescent organometallic complexes or fluorescent π -conjugated systems: indeed, blue emitters are currently a bottleneck in organic light-emitting diode (OLED) development.^{56,57}

Conflicts of interest

There are no conflicts to declare.

Acknowledgements

The work was funded by NSFC (No.51473028), the key scientific and technological project of Jilin province (20150204011GX, 20160307016GX, 20190701010GH), the Development and Reform Commission of Jilin province (20160058, 2020C035-5). M. R. B. thanks EPSRC grant EL/L02621X/1 for funding.

Notes and references

- Y. H. Kim, J. Y. Bae, J. Jin and B. S. Bae, *ACS Appl. Mater. Interfaces*, 2014, **6**, 3115-3121.
- R. Li, S. Wang, Q. Li, H. Lan, S. Xiao, Y. Li, R. Tan, T. Yi, *Dyes Pigm.*, 2017, **137**, 111-116.
- B. Xie, R. L. Parkhill, W. L. Warren and J. E. Smay, *Adv. Funct. Mater.*, 2006, **16**, 1685-1693.
- Z. Zhao, J. W. Y. Lamb and B. Z. Tang, *Soft Matter*, 2013, **9**, 4564-4579.
- H. Mehdi, H. Pang, W. Gong, M. K. Dhinakaran, A. Wajahat, X. Kuang and G. Ning, *Org. Biomol. Chem.*, 2016, **14**, 5956-5964.
- S. Chen, X. Luo, H. W. He, S. Chen, X. Q. Tong, Y. Chen, B. Z. Wu, M. Ma, X. Wang, *J. Mater. Chem. C*, 2015, **3**, 12026-12031.
- F. Chen, Y. M. Wang, W. Guo and X. B. Yin, *Chem. Sci.*, 2019, **10**, 1644-1650.
- Z. Li, G. Wang, Y. Wang and H. Li, *Angew. Chem. Int. Ed. Engl.*, 2018, **57**, 2194-2198.
- V. M. Suresh, A. De and T. K. Maji, *Chem. Commun.*, 2015, **51**, 14678-14681.
- B. Yuan, S. Guan, X. Sun, X. Li, H. Zeng, Z. Xie, P. Chen, S. Zhou, *ACS Appl. Mater. Interfaces*, 2018, **10**, 16005-16014.
- P. Xue, J. Ding, Y. Shen, H. Gao and J. Zhao, *Dyes Pigm.*, 2017, **145**, 12-20.

- 12 J.-Y. Lin, B. Liu, M.-N. Yu, C.-J. Ou, Z.-F. Lei, F. Liu, X.-H. Wang, L.-H. Xie, W.-S. Zhu, H.-F. Ling, X.-W. Zhang, P. N. Stavrinou, J.-P. Wang, D. D. C. Bradley and W. Huang, *J. Mater. Chem. C*, 2017, **5**, 6762-6770.
- 13 F. Gu, C. Zhang and X. Ma, *Macromol. Rapid Comm.*, 2019, **40**, 1800751.
- 14 H.-J. Kim, H. J. Lee, J. W. Chung, D. R. Whang and S. Y. Park, *Adv. Opt. Mater.*, 2018, **7**, 1801348.
- 15 P. R. A. Chivers and D. K. Smith, *Chem. Sci.*, 2017, **8**, 7218-7227.
- 16 Q. Zhu, L. Zhang, K. V. Vliet, A. Miserez and N. H. Andersen, *ACS Appl. Mater. Interfaces*, 2018, **10**, 10409-10418.
- 17 A. Kumar, A. Srivastava, I. Y. Galaev and B. Mattiasson, *Prog. Polym. Sci.*, 2007, **32**, 1205-1237.
- 18 F. Mo, H. Li, Z. Pei, G. Liang, L. Ma, Q. Yang, D. Wang, Y. Huang and C. Zhi, *Sci. Bull.*, 2018, **63**, 1077-1086.
- 19 F. Oroojalian, M. Babaei, S. M. Taghdisi, K. Abnous, M. Ramezani and M. Aliboland, *J. Control. Release*, 2018, **288**, 45-61.
- 20 G. Z. Zhao, L. J. Chen, W. Wang, J. Zhang, G. Yang, D. X. Wang, Y. Yu and H. B. Yang, *Chem.-Eur. J.*, 2013, **19**, 10094-10100.
- 21 Z. Zhang, Z. Wu, J. Sun, P. Xue and R. Lu, *RSC Adv.*, 2016, **6**, 43755-43766.
- 22 K. Y. Pu and B. Liu, *Adv. Funct. Mater.*, 2009, **19**, 277-284.
- 23 W. Che, G. Li, X. Liu, K. Shao, D. Zhu, Z. Su and M. R. Bryce, *Chem. Commun.*, 2018, **54**, 1730-1733.
- 24 Q. Zhou, B. Cao, C. Zhu, S. Xu, Y. Gong, W. Z. Yuan, Y. Zhang, *Small*, 2016, **12**, 6586-6592.
- 25 N. Jiang, G. F. Li, B. H. Zhang, D. X. Zhu, Z. M. Su and M. R. Bryce, *Macromolecules*, 2018, **51**, 4178-4184.
- 26 Q. Li and Z. Li, *Adv. Sci.*, 2017, **4**, 1600484.
- 27 J. Yang, J. Qin, P. Geng, J. Wang, M. Fang and Z. Li, *Angew. Chem. Int. Ed.*, 2018, **57**, 14174-14178.
- 28 Y. Jiang, G. Li, W. Che, Y. Liu, B. Xu, G. Shan, D. Zhu, Z. Su and M. R. Bryce, *Chem. Commun.*, 2017, **53**, 3022-3025.
- 29 B. Xu, M. Xie, J. He, B. Xu, Z. Chi, W. Tian, L. Jiang, F. Zhao, S. Liu, Y. Zhang, Z. Xu and J. Xu, *Chem. Commun.*, 2013, **49**, 273-275.
- 30 C. Yu, E. Hao, X. Fang, Q. Wu, L. Wang, J. Li, L. Xu, L. Jiao, W.-Y. Wong, *J. Mater. Chem. C*, 2019, **7**, 3269-3277.
- 31 P. Chen, Q. Li, S. Grindy and N. H. Andersen, *J. Am. Chem. Soc.*, 2015, **137**, 11590-11593.
- 32 T. Mondal, T. Sakurai, S. Yoneda, S. Seki and S. Ghosh, *Macromolecules*, 2015, **48**, 879-888.
- 33 Y.-C. Tsai, S. Li, S.-G. Hu, W.-C. Chang, U.-S. Jeng and S.-H. Hsu, *ACS Appl. Mater. Interfaces*, 2015, **7**, 27613-27623.
- 34 Y.-S. Ren, S. Xie, E.S. Grape, A. K. Inge, O. Ramström, *J. Am. Chem. Soc.*, 2018, **140**, 42, 13640-13643.
- 35 D. D. Prabhu, N. S. S. Kumar, A. P. Sivasadas, S. Varghese, S. Das, *J. Phys. Chem. B*, 2012, **116**, 43, 13071-13080.
- 36 M. Sun, L. Zhai, J. Sun, F. Zhang, W. Mi, J. Ding, R. Lu, *Dyes Pigm.*, 2019, **162**, 67-74.
- 37 M. Luo, S. Wang, C. Li, W. Miao, X. Ma, *Dyes Pigm.*, 2019, **165**, 436-443.
- 38 X. Wu, Y. Wu, C. Zhang, H. Niu, L. Lei, C. Qin, C. Wang, X. Bai and W. Wang, *RSC Adv.*, 2015, **5**, 58843-58853.
- 39 S. Niu, H. Yan, *Macromol. Rapid. Commun.*, 2015, **36**, 739-743.
- 40 S. Niu, H. Yan, S. Li, C. Tang, Z. Chen, X. Zhi and P. Xu, *J. Mater. Chem. C.*, 2016, **4**, 6881-6893.
- 41 C. Liu, H. Qin and P. T. Mather, *J. Mater. Chem.*, 2007, **17**, 1543-1558.
- 42 D. K. Chattopadhyay and K. V. S. N. Raju, *Prog. Polym. Sci.*, 2007, **32**, 352-418.
- 43 A. Lendlein and S. Kelch, *Angew. Chem. Int. Ed.*, 2002, **41**, 2034-2057.
- 44 W. Sun, Z. Wang, T. Wang, L. Yang, J. Jiang, X. Zhang, Y. Luo, G. Zhang, *J. Phys. Chem. A*, 2017, **121**, 4225-4232.
- 45 Q. Wan, M. Liu, L. Mao, R. Jiang, D. Xu, H. Huang, Y. Dai, F. Deng, X. Zhang and Y. Wei, *Mat. Sci. Eng. C*, 2017, **72**, 352-358.
- 46 W. Yu, Y. Wu, J. Chen, X. Duan, X. F. Jiang, X. Qiu, Y. Li, *RSC Adv.*, 2016, **6**, 51257-51263.
- 47 E. Rideau, R. Dimova, P. Schwille, F. R. Wurm and K. Landfester, *Chem. Soc. Rev.*, 2018, **47**, 8572-8610.
- 48 A. Ajayaghosh, R. Varghese, S. Mahesh and V. K. Praveen, *Angew. Chem., Int. Ed.*, 2006, **45**, 7729-7732.
- 49 R. Chapman, M. Danial, M. L. Koh, K. A. Jolliffe and S. Perrier, *Chem. Soc. Rev.*, 2012, **18**, 6023-6041.
- 50 H. Shao, J. Seifert, N. C. Romano, M. Gao, J. J. Helmus, C. P. Jaroniec, D. A. Modarelli and J. R. Parquette, *Angew. Chem., Int. Ed.*, 2010, **49**, 7688-7691.
- 51 S. Tu, S. H. Kim, J. Joseph, D. A. Modarelli and J. R. Parquette, *J. Am. Chem. Soc.*, 2011, **133**, 19125-19130.
- 52 M. J. Robb, D. Montarnal, N. D. Eisenmenger, S. Y. Ku, M. L. Chabincyc and C. J. Hawker, *Macromolecules*, 2013, **46**, 6431-6438.
- 53 K. Kojio, S. Nakashima and M. Furukawa, *Polymer*, 2007, **48**, 997-1004.
- 54 D. R. Canchi, D. Paschek, and A. E. García, *J. Am. Chem. Soc.*, 2010, **132**, 2338-2344.
- 55 M. A. Corcuera, L. Rueda, A. Saralegui, M. D. Martín, B. F. d'Arlas, I. Mondragon, *J. Appl. Polym. Sci.*, 2011, **122**, 3677-3685.
- 56 X. Yang, X. Xu and G. Zhou, *J. Mater. Chem. C*, 2015, **3**, 913-944.
- 57 J.-H. Lee, C.-H. Chen, P.-H. Lee, H.-Y. Lin, M.-k. Leung, T.-L. Chiu and C.-F. Lin, *J. Mater. Chem. C*, 2019, **7**, 5874-5888.

Supporting Information

Blue-emitting thermoreversible oligourethane gelators with aggregation-induced emission properties

Nan Jiang, Dongxia Zhu,^{a,*} Zhongmin Su^{a,*} and Martin R. Bryce^{b,*}

^a Key Laboratory of Nanobiosensing and Nanobioanalysis at Universities of Jilin Province, Department of Chemistry, Northeast Normal University, 5268 Renmin Street, Changchun, Jilin Province 130024, P. R. China.

^b Department of Chemistry, Durham University, Durham, DH1 3LE, UK.

Table of Contents:	Page
1. Experimental details	2
2. Structural characterization of OUs	3
3. Photophysical properties of OUs	7

1. Experimental details

General:

Materials obtained from commercial suppliers were used without further purification unless otherwise stated. All glassware, syringes, magnetic stirring bars and needles were thoroughly dried in a convection oven. ^1H NMR spectra were recorded at 25 °C on a Varian 500 MHz spectrometer and were referenced internally to the residual proton resonance in $\text{DMSO-}d_6$ (δ 2.5 ppm). The molecular weights of the oligomers were calculated from their ^1H NMR spectra, as described in the sections below. UV-vis absorption spectra were recorded on a Shimadzu UV-3100 spectrophotometer. Photoluminescence spectra were collected on an Edinburgh FLS920 spectrophotometer.

Synthesis of OU Derivatives:

OU Derivatives were synthesized according to a similar method used in previous work.¹

OUHDI. A mixture of 4,4'-sulfonyldiphenol (2.62 mmol), polyethylene glycol mono-methyl ether ($M_w = 200 \text{ g mol}^{-1}$; 1.98 mmol), anhydrous acetonitrile (8 mL), hexamethylene diisocyanate (3.61 mmol) and DABCO (0.105 mmol) were added to a dried two-neck round-bottom flask. The solution was heated at 75 °C for 8 h under nitrogen atmosphere. After the clear solution became significantly viscous, the product was precipitated from excess diethyl ether. Then the product was dried under vacuum for 24 h to obtain **OUHDI**. Yield: 69%. ^1H NMR (500 MHz, $\text{DMSO-}d_6$, δ [ppm]): 7.1-8.0 (broad, 8H; 4,4'-sulfonyldiphenol protons), 6.9 (broad, 4H), 4.03 (s, 4H), 3.4-3.68 (broad, PEG protons), 3.3 (s, 3H; PEG terminal $-\text{OCH}_3$ protons), 3.1-2.9 (broad, 4H), 1.2-1.6 (broad, 4H). FTIR: 3342 cm^{-1} (N-H), 2858 and 2933 cm^{-1} ($-\text{CH}_2-$ asymmetric and symmetric stretch), 1712 cm^{-1} (C=O), 1105 cm^{-1} (C-O-C stretch PEG). $M_w = 4192 \text{ g mol}^{-1}$.

OUHMDI. The synthetic procedure for **OUHMDI** was the same as **OUHDI**, except monomer methylene-bis(4-cyclohexyl isocyanate) was used instead of hexamethylene diisocyanate. Yield: 65%. ^1H NMR (500 MHz, $\text{DMSO-}d_6$, δ [ppm]): 7.25-8.0 (broad, 8H; 4,4'-sulfonyldiphenol protons), 6.85 (broad, 2H), 3.85 (s, 2H), 4.05 (s, 2H), 3.40-3.60 (broad, PEG protons), 3.25 (s,

3H; PEG terminal $-OCH_3$ protons), 2.5-1.20 (broad, 10H). FTIR: 3313 cm^{-1} (N-H), 2856 and 2930 cm^{-1} ($-CH_2-$ asymmetric and symmetric stretching), 1703 cm^{-1} (C=O), 1106 cm^{-1} (C-O-C stretching PEG). $M_w = 1749\text{ g mol}^{-1}$.

OUTDI. The synthetic procedure for **OUTDI** was the same as **OUHDI**, except monomer 2,4-diisocyanatotoluene was used instead of hexamethylene diisocyanate. Yield: 63%. $^1\text{H NMR}$ (500 MHz, $\text{DMSO-}d_6$, δ [ppm]): 8.85-9.0 (broad, 2H), 6.55-8.0 (broad, 8H; 4,4-sulfonyldiphenol protons), 4.2 (s, 4H), 3.45-3.7 (broad, PEG protons), 3.4 (s, 3H; PEG terminal $-OCH_3$ protons), 1.95-2.25 (broad, 3H). FTIR: 3305 cm^{-1} (N-H), 2873 and 2937 cm^{-1} ($-CH_2-$ asymmetric and symmetric stretching), 1736 cm^{-1} (C=O), 1104 cm^{-1} (C-O-C stretching PEG). $M_w = 2775\text{ g mol}^{-1}$.

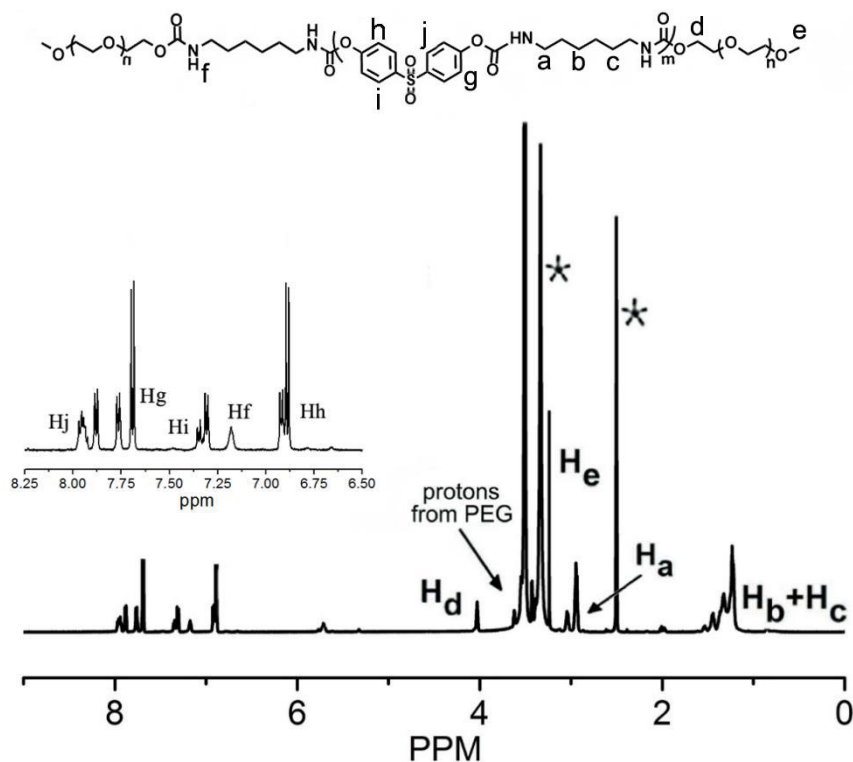


Fig. S1 $^1\text{H NMR}$ spectrum of **OUHDI** in $\text{DMSO-}d_6$ (* indicates peaks from the solvent and water)

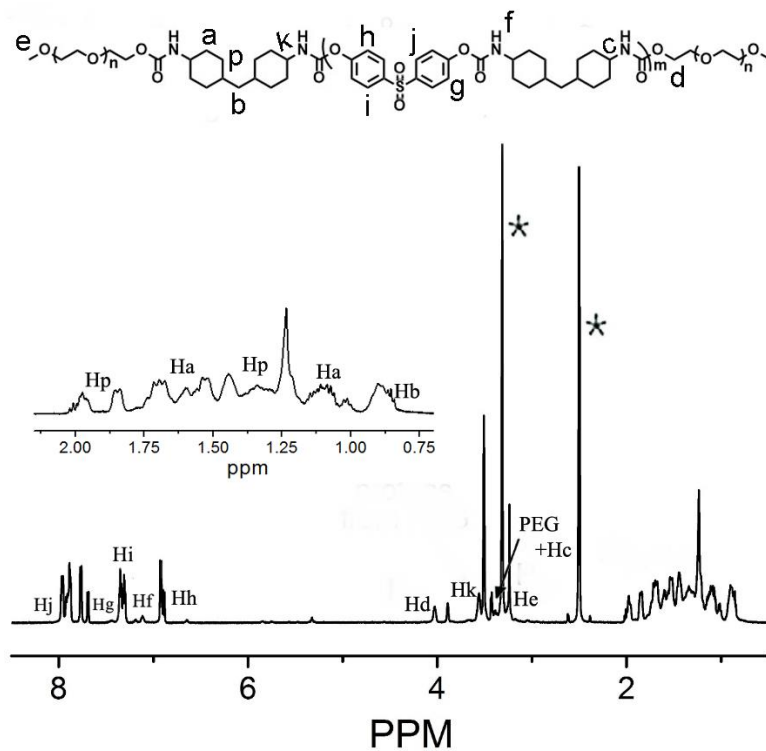


Fig. S2 ¹H NMR spectrum of **OUHMIDI** in DMSO-*d*₆ (* indicates peaks from the solvent and water)

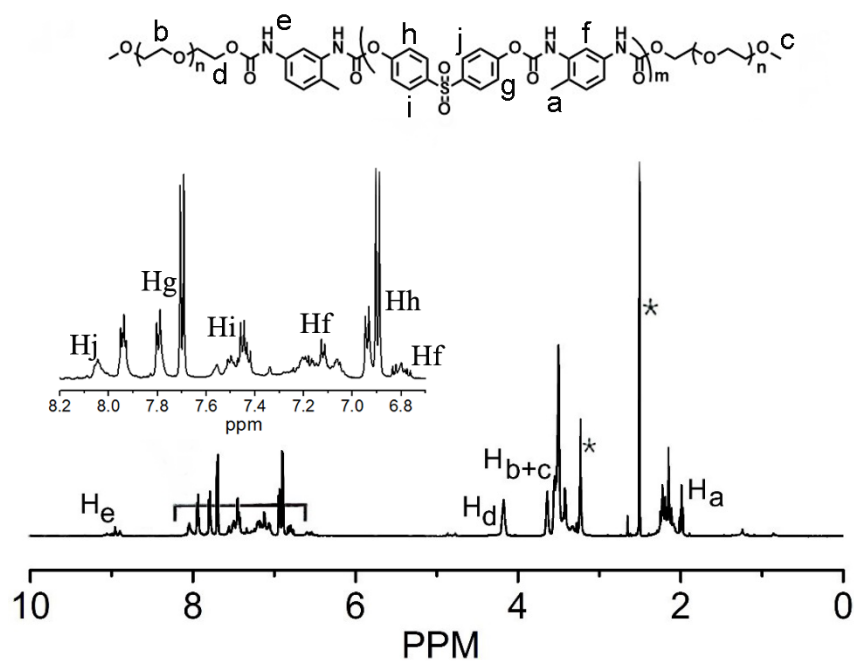
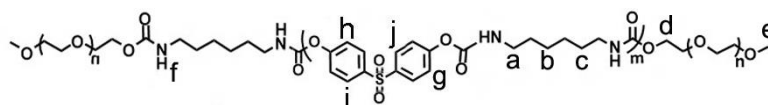


Fig. S3 ¹H NMR spectrum of **PUTDI** in DMSO-*d*₆ (* indicates peaks from the solvent and water)

Molecular Weight Calculation:

For co-polymers and oligomers with higher polarity, it is difficult to find a suitable standard solution for determining their molecular weights by gel permeation chromatography (GPC) experiments. Therefore, nuclear magnetic resonance (NMR) spectroscopy is often used to calculate the number-average molecular weight.² Specifically, end-substituent analysis is used to compare the integral values of the polymer end-substituent and the characteristic peaks of the main chain repeat element. In this way the average number of repeat units (degree of polymerization), and hence the molecular weight of polymer are calculated. The premise is to assume that each chain has the same end group at both ends. Low molecular weight polymers and oligomers give accurate results, but the data will be less accurate for higher molecular weights. This method requires the unambiguous assignment of specific protons in the ¹H NMR spectrum. The integral ratio of different characteristic peaks and terminal groups was used to calculate the number of repeat units in the oligomer chains.



For example, in **OUHDI**, the characteristic peaks of hydrogens in the main chains (Ha/Hh) and the methyl end group (He) were chosen to calculate the integral ratio and obtain the degree of polymerization (m). In addition, 'n' is known. Finally, the molecular weight can be obtained by adding up each of these parts.

Gelation studies:

The OU (8 wt %) was dissolved in *N,N*-dimethylformamide (DMF) under heating. A clear solution was obtained and allowed to cool down to room temperature. After 10-20 min, a transparent gel formed. Similar experiments done with dimethyl sulfoxide (DMSO), or dimethylacetamide (DMAc) solvent, gave spontaneous gelation in all cases.

Determination of Critical Gelation Concentration:

The PU (8 wt%) was gradually added to a measured amount of DMF and heated to make a clear solution. Gelation was confirmed by an inversion method after 10 min. Up to a certain

concentration, gelation was noticed, which even after a prolonged wait, no gelation occurred. This concentration is considered as a critical gelation concentration.

Determination of T_{gel} :

A closed vial containing the gel was placed on a digital display heater. The temperature was gradually increased from 20 °C, and the existence of the gel was examined by tilting the vial. At a given temperature, the gel no longer was stable when the vial was inverted. This temperature was recorded as the gel-to-sol melting temperature (T_{gel}).

Rheological Experiments:

Gels (8 wt%) were prepared and stored at room temperature for 12 h before rheological experiments were performed in an Anton-Paar MCR 302 rheometer. Stress-amplitude sweep measurements were used to record the gel strength. The runs were carried out at a constant oscillation frequency of 1 Hz at 25 °C.

Urea Addition Experiments:

Gels (8 wt %) were prepared in DMF and then urea (10 eq.) was added to the gel vial, and then the mixture was heated to make a clear solution and then cooled to room temperature. It was observed that after urea addition the gel did not form again.

The preparation method of films:

3.5 wt% of **OUHDI** sol was poured on a PTFE board, and placed under vacuum several times to remove all the air bubbles. The sample was then heated at 60 °C for 4 h and dried in a vacuum oven.

The preparation method of stereoscopic molds:

A small amount of **OUHDI** powder was placed in a vial and a few drops of DMF were added to the vial. Heating the mixture with a hair-dryer quickly dissolved the powder. The cycle of adding more **OUHDI** powder and heating was repeated a few times until a sticky gel appeared in the bottom of the vial. This sticky gel was then placed in the mold using a plastic dropper.

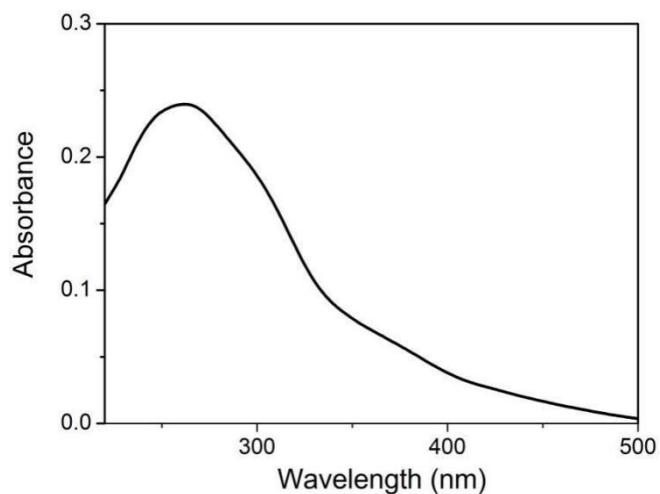


Fig. S4 Absorption spectrum of **OUHDI** in the solid state.

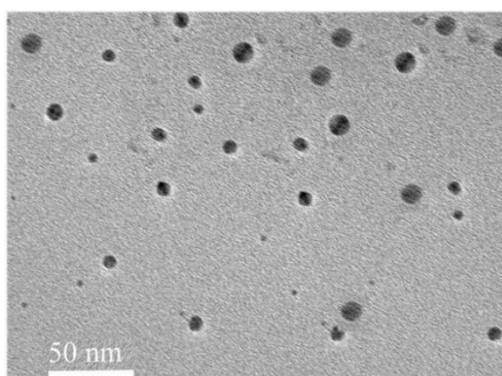


Fig. S5 TEM image of nanoaggregates of **OUHDI** formed in acetone- H_2O mixture with 90% water fraction (10^{-5} M).

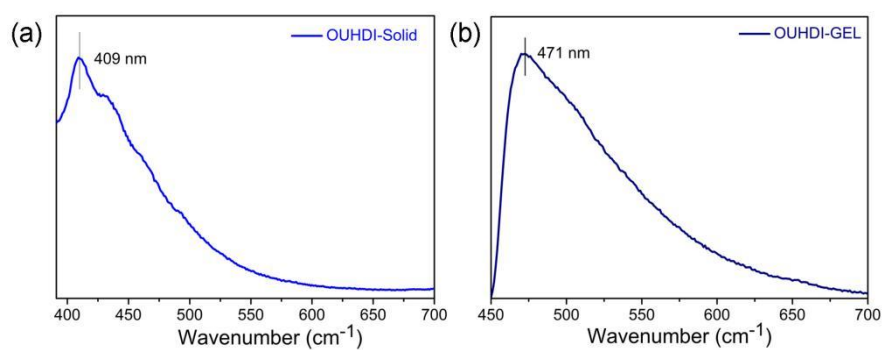


Fig. S6 (a) PL spectra of **OUHDI** solid. (b) PL spectra of **OUHDI** gel. ($\lambda_{\text{ex}} = 365$ nm)

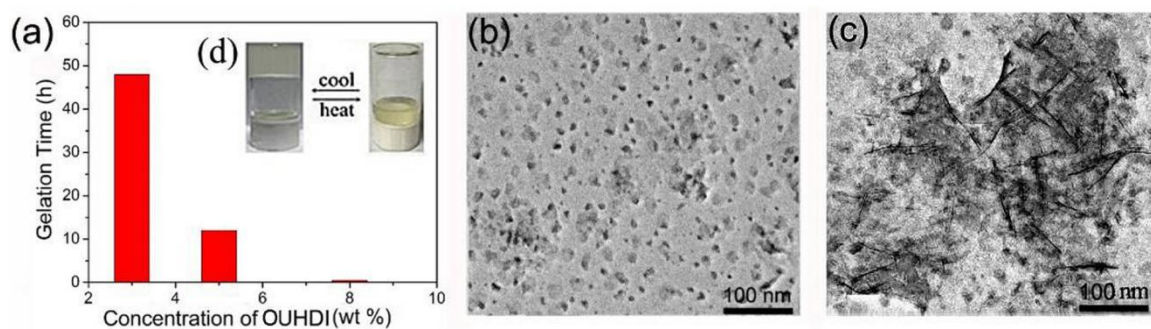


Fig. S7 (a) Variation of gelation time with concentration of **OUHDI**. TEM images of (b) freshly prepared solution and (c) aged (48 h, room temperature) gel of **OUHDI** in DMF ($c = 0.2$ wt %). (d) sol-gel transition of **OUHDI** in DMF.

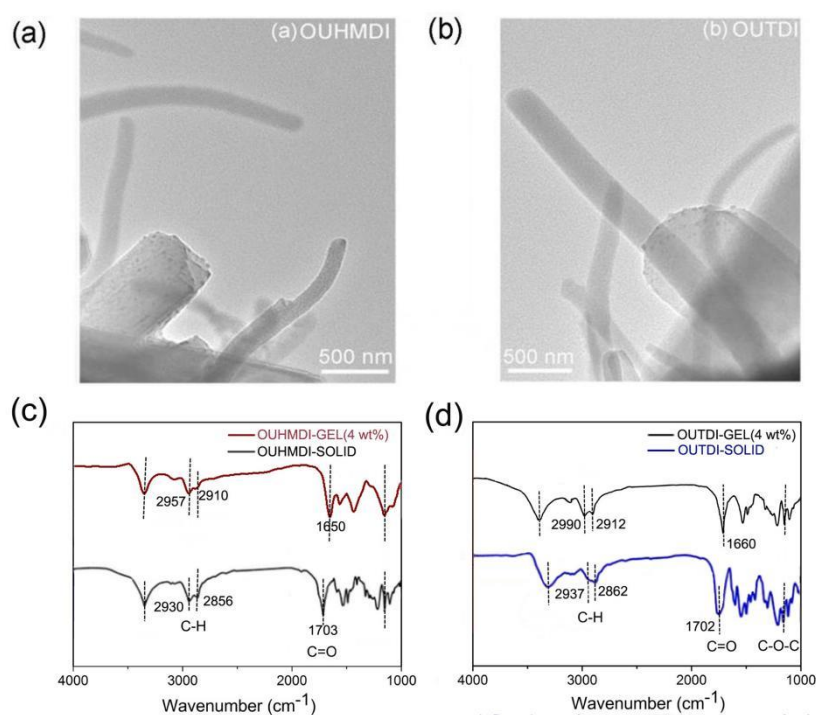


Fig. S8 TEM images of nanotubes (a) **OUHMDI** (b) **OUTDI** formed in 0.8 wt% DMF solution. (c) FTIR spectra of **OUHMDI** in solid and gel states. (d) FTIR spectra of **OUTDI** in solid and gel states.

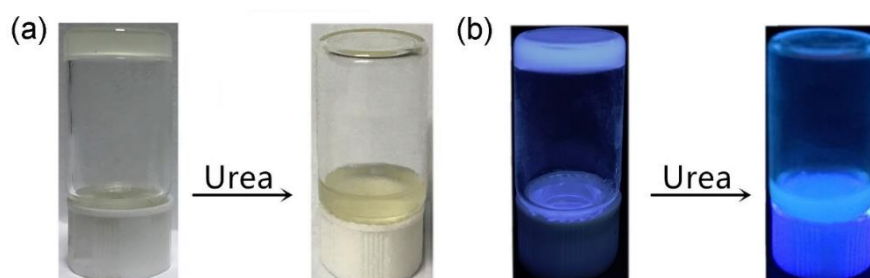


Fig. S9 Urea (10 eq. with respect to the repeat unit of OU) mediated gel-to-sol transformation of **OUHDI** gel in DMF under (a) sunlight (b) UV light.

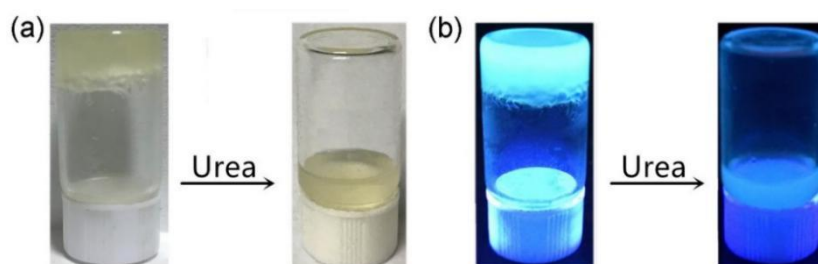


Fig. S10 Urea (10 eq. with respect to the repeat unit of OU) mediated gel-to-sol transformation of **OUHMDI** gel in DMF under (a) sunlight (b) UV light.

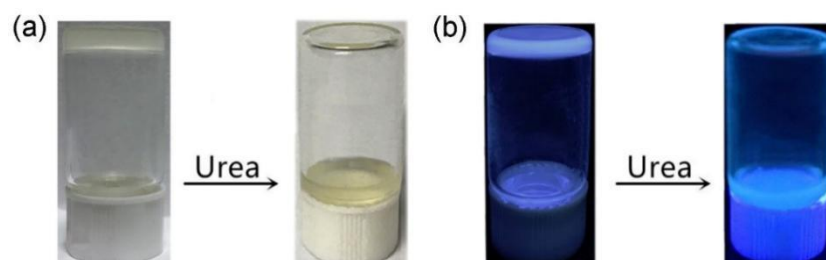


Fig. S11 Urea (10 eq. with respect to the repeat unit of the OU) mediated gel-to-sol transformation of **OUTDI** gel in DMF under (a) sunlight (b) UV light.

Table S1: Observation of gelation tests of **OUs** in different solvents ($c = 8$ wt%).

DMF	DMSO	DMAC	CHCl ₃	THF	MCH	Acetone
Gel	Gel	Gel	Sol	Sol	Precipitate	Sol

Table S2: Gelation Data of the OUs.

Oligourethane	CGC (wt %)	T_{gel} ($^{\circ}$ C) ^a	ΔH_{m} (kJ mol^{-1})	G' (Pa)	G'' (Pa)	σ (Pa)
OUHDI	3.5	99	20.3	101.3	1.2	1.5
OUHMDI	4	96	18.4	83.0	17	0.7
OUTDI	4.3	83	15.0	28.1	2.4	0.5

^a Concentration of gelator = 8 wt%

References

- 1 N. Jiang, G. F. Li, W. L. Che, D. X. Zhu, Z. M. Su and M. R. Bryce, *J. Mater. Chem. C*, 2018, **6**, 11287-11291.
- 2 T. F. Page, W. E. Bresler, *Anal. Chem.*, 1964, **10**, 1981-1985.